

## Ultrasonic Measurement of Strain Distribution Inside Object Cyclically Compressed by Dual Acoustic Radiation Force

Yoshitaka ODAGIRI, Hideyuki HASEGAWA, and Hiroshi KANAI\*

Graduate School of Engineering, Tohoku University, Sendai 980-8579, Japan

(Received November 26, 2007; revised February 23, 2008; accepted March 3, 2008; published online May 23, 2008)

One possible way to evaluate acupuncture therapy quantitatively is to measure the change in the elastic property of muscle after application of the therapy. Many studies have been conducted to measure mechanical properties of tissues using ultrasound-induced acoustic radiation force. To assess mechanical properties, strain must be generated in an object. However, a single radiation force is not effective because it mainly generates translational motion when the object is much harder than the surrounding medium. In this study, two cyclic radiation forces are simultaneously applied to a muscle phantom from two opposite horizontal directions so that the object is cyclically compressed in the horizontal direction. By the horizontal compression, the object is expanded vertically based on its incompressibility. The resultant vertical displacement is measured using another ultrasound pulse. Two ultrasonic transducers for actuation were both driven by the sum of two continuous sinusoidal signals at two slightly different frequencies [1 MHz and (1 M + 5) Hz]. The displacement of several micrometers in amplitude, which fluctuated at 5 Hz, was measured by the ultrasonic *phased tracking method*. Increase in thickness inside the object was observed just when acoustic radiation forces increased. Such changes in thickness correspond to vertical expansion due to horizontal compression. [DOI: 10.1143/JJAP.47.4193]

KEYWORDS: acoustic radiation force, phased tracking method, acupuncture therapy, strain

### 1. Introduction

Acupuncture was first used more than 2,000 years ago and has been developed based on the results of experience. However, the mechanism by which acupuncture therapy works is not clearly understood. Therefore, the quantitative evaluation of acupuncture therapy is important and the measurement of changes in elastic properties of muscle due to treatments is one of the strategies for quantitative evaluation of the therapy. When acupuncture is effective, the elastic modulus of muscle after acupuncture therapy decreases compared with that before therapy.

Recently, some remote actuation methods based on acoustic radiation forces have been reported. Fatemi and Greenleaf proposed an imaging modality that uses the acoustic response of an object to a localized dynamic radiation force.<sup>1,2)</sup> The radiation force produces an acoustic emission which is closely related to the mechanical frequency response of the medium. By measuring the acoustic emission with a hydrophone, hard inclusions such as calcified tissues in soft material were detected experimentally. The spatial resolution in the depth direction corresponds to the size of the intersectional area of ultrasound beams at two different frequencies.

Nightingale *et al.* proposed an alternative imaging method in which focused ultrasound is employed to apply the radiation force to soft tissue for short durations (less than 1 ms). The viscoelastic properties of the tissue were investigated from the magnitude of the transient response, which was measured as the displacement,  $d(t)$ , of the tissue.<sup>3–5)</sup> In order to generate measurable  $d(t)$  using several ultrasonic pulses, high-intensity pulsed ultrasound (1,000 W/cm<sup>2</sup>) was employed. According to safety guidelines for the use of ultrasound, the intensity is recommended to be below 240 mW/cm<sup>2</sup> for pulsed waves and 1 W/cm<sup>2</sup> for the continuous waves.<sup>6)</sup> Therefore, the intensity of the pulsed ultrasound employed by Nightingale

*et al.* would be far greater than that indicated in the safety guidelines.

Acoustic radiation force has possibilities for use in the measurement of mechanical properties of tissues. However, a single acoustic radiation force does not generate strain in an object effectively because it primarily produces a change in the object's position which has zero spatial gradient in displacement (no strain). Specifically when the elastic modulus of the object is far greater than that of the surrounding medium, a single acoustic radiation force may generate only a change in the position of the object. To effectively generate strain in the object, Hasegawa *et al.* used two acoustic radiation forces.<sup>7)</sup> Two sets of cyclically oscillating acoustic radiation forces induced by two ultrasounds at frequencies  $f$  and  $f + \Delta f$  were simultaneously applied to two different positions in the object from two different directions. In this case, two ultrasound beams crossed each other at certain depth from the surface as shown in Fig. 1, and the shadowed region that compressed horizontally corresponded to the generation of strain.

In our previous studies,<sup>7,8)</sup> ultrasound at 1 MHz and 5 MHz was used for actuation and measurement, respectively. Therefore, irradiation of ultrasound for actuation needed to be stopped during transmission and reception of ultrasound for measurement because the frequencies of these two ultrasounds is insufficiently different, and it is difficult to separate them by filtering. In this study, continuous ultrasound for actuation was used to obtain a larger amplitude of displacement in comparison with that in previous studies. In order to separate the pulsed ultrasound for the measurement from the continuous ultrasound for actuation by filtering, high-frequency ultrasound was employed (center frequency: 16 MHz) for measurement of displacements. Using this newly developed experimental system, an object was stably actuated by two acoustic radiation forces with a larger amplitude, and the change in thickness (= strain) inside the object was imaged at a high spatial resolution by the ultrasonic *phased tracking method*.<sup>9,10)</sup>

\*E-mail address: hkanai@ecei.tohoku.ac.jp

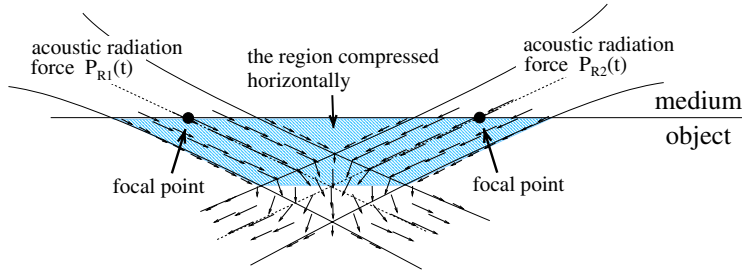


Fig. 1. (Color online) Illustration of acoustic radiation forces generated by two ultrasound beams focused at two points separated by a given distance.

### 2. Principles

When ultrasound propagates in a medium (density:  $\rho_1$ , sound speed:  $c_1$ ), a constant force is generated in the direction of propagation. This force is called the acoustic radiation force.<sup>11)</sup> The acoustic radiation pressure,  $P_R(t)$ , is defined as the acoustic radiation force per unit area as follows:

$$P_R(t) = (1 + R^2)e(t), \tag{2.1}$$

where  $R$  and  $e(t)$  are the pressure reflection coefficient and the energy density at the interface between the medium and object, respectively. In eq. (2.1), the transmitted wave is assumed to be perfectly absorbed by the object. Using the densities,  $\rho_1$  and  $\rho_2$ , and sound speed,  $c_1$  and  $c_2$ , of the medium, the reflection coefficient,  $R$ , and the energy density,  $e(t)$ , are defined by

$$R = \frac{Z_2 - Z_1}{Z_2 + Z_1} = \frac{\rho_2 c_2 - \rho_1 c_1}{\rho_2 c_2 + \rho_1 c_1}, \tag{2.2}$$

$$e(t) = \frac{1}{\rho_1 c_1^2} [p(t)]^2. \tag{2.3}$$

For example, the speed of sound in muscle and fat are 1,568 and 1,465 m/s, respectively. By assuming densities of these tissue to be  $1.0 \times 10^3 \text{ kg/m}^3$ , the reflection coefficient  $R$  is 0.034. Thus, the square of the reflection coefficient,  $R^2$ , is assumed to be zero. The energy density,  $e(t)$ , of the incident wave is proportional to the square of the sound pressure,  $p(t)$ , of the ultrasound beam. When two ultrasound waves with the same sound pressure,  $p_0$ , at slightly different frequencies,  $f$  and  $f + \Delta f$ , are crossed each other, an acoustic radiation pressure,  $P_R(t)$ , which fluctuates at the frequency difference,  $\Delta f$ , is generated in the intersectional area. In this case, the sound pressure,  $p_{\text{sum}}(t)$ , in the intersectional area is expressed as follows:

$$p_{\text{sum}}(t) = p_0 \cos 2\pi ft + p_0 \cos 2\pi(f + \Delta f)t, \tag{2.4}$$

and the energy density,  $e(t)$ , is given by

$$\begin{aligned} e(t) &= \frac{1}{\rho_1 c_1^2} [p_{\text{sum}}(t)]^2 \\ &= \frac{1}{\rho_1 c_1^2} [p_0 \cos 2\pi ft + p_0 \cos 2\pi(f + \Delta f)t]^2 \\ &= \frac{p_0^2}{\rho_1 c_1^2} \left[ 1 + \cos 2\pi \Delta f t + \cos 2\pi(2f + \Delta f)t \right. \\ &\quad \left. + \frac{1}{2} \cos 4\pi ft + \frac{1}{2} \cos 4\pi(f + \Delta f)t \right], \end{aligned} \tag{2.5}$$

From the second term on the right-hand side of eq. (2.5), it is found that the energy density,  $e(t)$ , has a component at the frequency difference  $\Delta f$ . With respect to the low-frequency component, the acoustic radiation pressure,  $P_R(t)$ , acting on the interface is given by

$$\begin{aligned} P_R(t) &= (1 + R^2) \frac{p_0^2}{\rho_1 c_1^2} (1 + \cos 2\pi \Delta f t) \\ &\simeq \frac{p_0^2}{\rho_1 c_1^2} (1 + \cos 2\pi \Delta f t). \end{aligned} \tag{2.6}$$

To improve the spatial resolution in measurements of the response of an object, an ultrasound correlation-based method, the ultrasonic *phased tracking method*, is used to measure the minute displacement,  $d(t)$ , caused by the acoustic radiation force.<sup>8)</sup> The accuracy of the displacement measurement by the *phased tracking method* was determined to be  $0.2 \mu\text{m}$  by basic experiments using a rubber plate.<sup>12)</sup> In addition, the *phased tracking method* has already been applied to measurements of vibrations and viscoelasticity of the arterial wall<sup>13,14)</sup> and heart wall.<sup>15,16)</sup>

### 3. Experimental Methods

The experimental setup is illustrated in Fig. 2. In order to measure the displacement distribution at a high spatial resolution, we employed ultrasonic diagnostic equipment (Dynamic Imaging DIASUS) with a linear probe (center frequency: 16 MHz). The equipment was modified to detect minute displacement in the object by the ultrasonic *phased tracking method*. A homogeneous object made of gel ( $45 \times 45 \times 17 \text{ mm}^3$ , static elastic modulus  $E_s$ : 6.3 kPa, containing 5% carbon powder by weight to provide

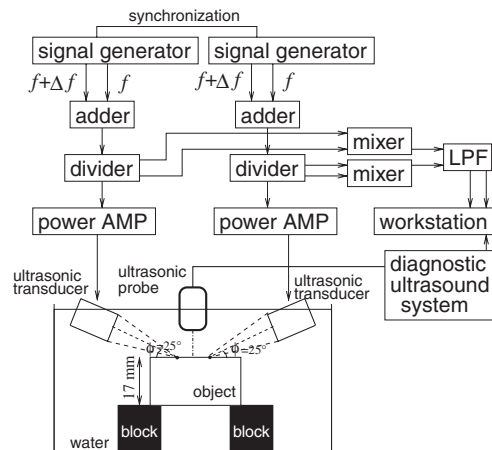


Fig. 2. Experimental setup for measurement of the displacement of an object cyclically actuated by ultrasound.

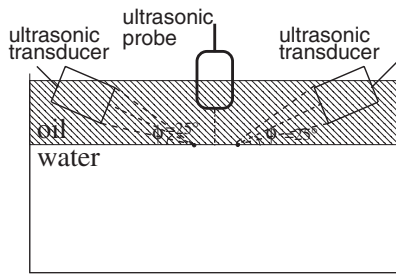


Fig. 3. Measurement of the interface between oil and water actuated by radiation forces.

sufficient scattering) was placed in a water tank as shown in Fig. 2. To apply radiation pressures  $P_{R1}(t)$  and  $P_{R2}(t)$ , two concave ultrasonic transducers were employed. Each concave ultrasonic transducer (center frequency: 1 MHz, focal length: 52 mm) was driven by the sum of two continuous waves (CWs) at two slightly different frequencies of 1 MHz and 1 MHz + 5 Hz. The resultant ultrasound beam was focused 50 mm away from the surface of the transducer, and the focal point was set at the top surface of the object at  $25^\circ$  in beam angle from the horizontal direction.

Ultrasound signals for actuation (around 1 MHz) received by the linear-array probe were filtered to estimate the displacement distribution using only the pulsed ultrasound for measurement (center frequency: 16 MHz).

#### 4. Results

##### 4.1 Displacement measurement at the boundary of oil and water

As illustrated in Fig. 3, the interface between oil and water was measured with ultrasound because the interface of liquids is easily actuated in large amplitude, and the actuated region can be easily identified. In this experiment, beam angles of two ultrasound waves for actuation were set to  $25^\circ$ , and the distance between two focal points was set to 16 mm. Figure 4 shows the sound field of the ultrasonic transducer used for actuation. Figures 4(b) and 4(c) show the measured sound pressure distribution in the depth and radial directions, respectively. From these results, the width,  $\Delta z_p$ , at half maximum of the sound pressure is determined to be about 2.5 mm along the  $x$ -axis ( $z = 52$  mm).

Figure 5 shows the displacement of each beam for measurement during a cycle of acoustic radiation forces. The time of the measured displacement relative to acoustic radiation forces is shown in Fig. 5(b). In Fig. 5(a), measured displacements are superimposed on the B-mode images using a color code shown in the bottom of Fig. 5. Blue and red correspond to downward and upward displacement of the interface, respectively. In Fig. 5, the downward displacement around focal points of ultrasound for actuation during the increase in acoustic radiation forces is clearly visualized, and the regions through which acoustic radiation forces pass can be easily recognized. The regions showing downward displacement during the increase of applied acoustic radiation forces are wider than  $\Delta z_p$  of the sound pressure distribution shown in Fig. 4(c) because ultrasound beams for actuation were insonified at an angle of  $25^\circ$  between the interface and beam, and the beam diameter on the interface was wider than  $\Delta z_p$ .

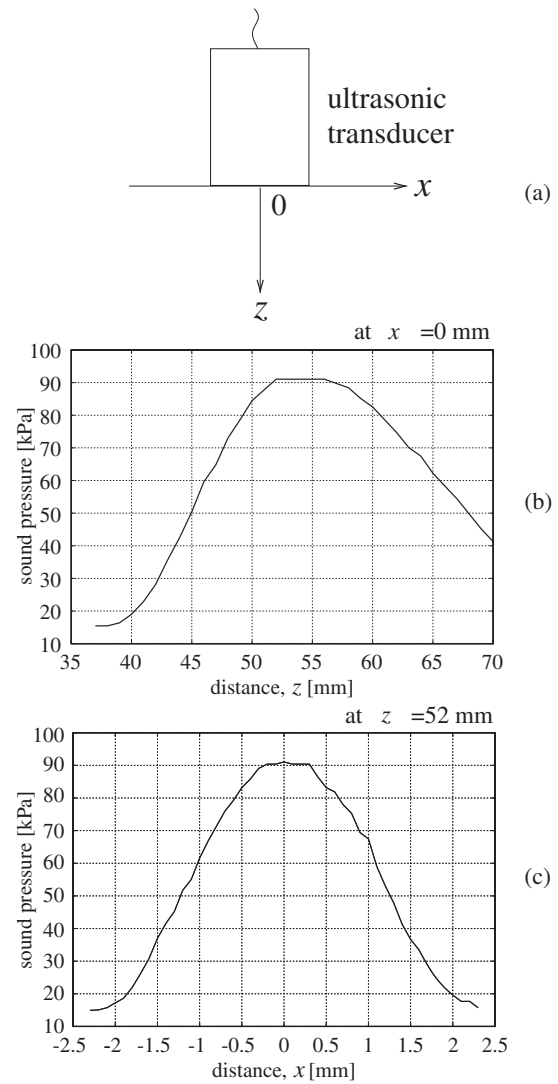


Fig. 4. (a) Measurement axis of sound pressure of an ultrasonic transducer used for actuation. (b) Sound pressure distribution in the depth direction at  $x = 0$  mm. (c) Sound pressure distribution in the radial direction at  $z = 52$  mm.

##### 4.2 Displacement measurement inside the object

When two acoustic radiation forces were applied to two different positions in the object from two different directions, acoustic radiation forces overlap inside an object made of gel. The spatial distribution of displacements inside the object was measured with ultrasound. In this experiment, the distance between two focal points was set to 0 and 8 mm. Figure 6(a) shows an M-mode image of the object along the  $z$ -axis at the center ( $x = 0$ ) of two focal points. In Fig. 6, the distance between two focal points was set to 0 mm. Acoustic radiation pressures,  $P_{R1}(t)$  and  $P_{R2}(t)$ , shown in Figs. 6(b) and 6(c) were calculated based on eq. (2.6) as follows: The density,  $\rho_2$ , and the sound speed,  $c_2$ , of the object were measured as  $1.1 \times 10^3$  kg/m<sup>3</sup> and  $1.47 \times 10^3$  m/s, respectively, and the pressure reflection coefficient,  $R$ , and the energy reflection coefficient,  $R^2$ , were calculated as 0.038 and 0.0014 ( $\approx 0$ ), respectively, using eq. (2.2). In this study, by assuming the object to be a totally absorbing material, the acoustic radiation pressures,  $P_{R1}(t)$  and  $P_{R2}(t)$ , were calculated based on eq. (2.6). By measuring the acoustic field of

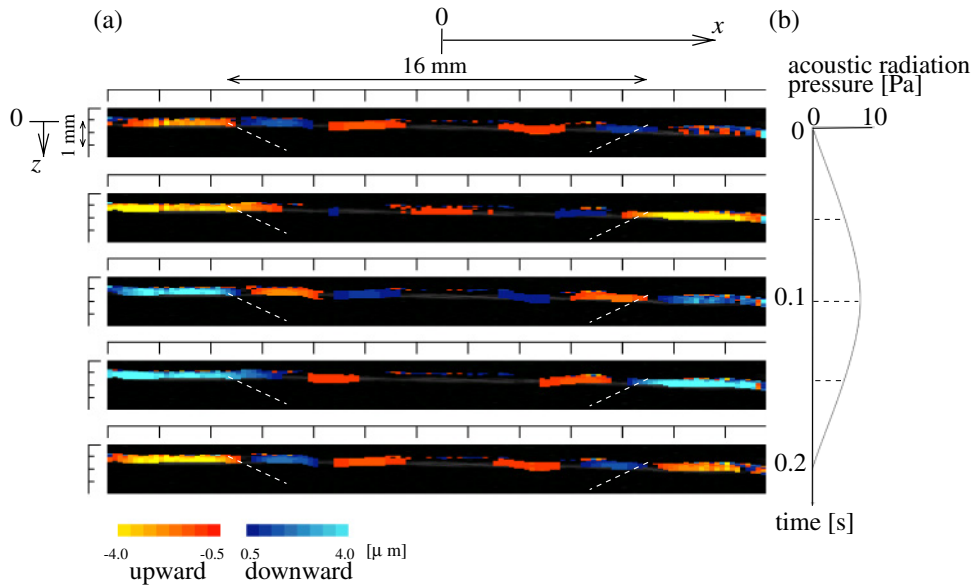


Fig. 5. (Color online) (a) Displacement distribution at the interface between oil and water successfully obtained every 50 ms during one cycle of the actuation from the top panel to the bottom panel. (b) Acoustic radiation force during the same period.

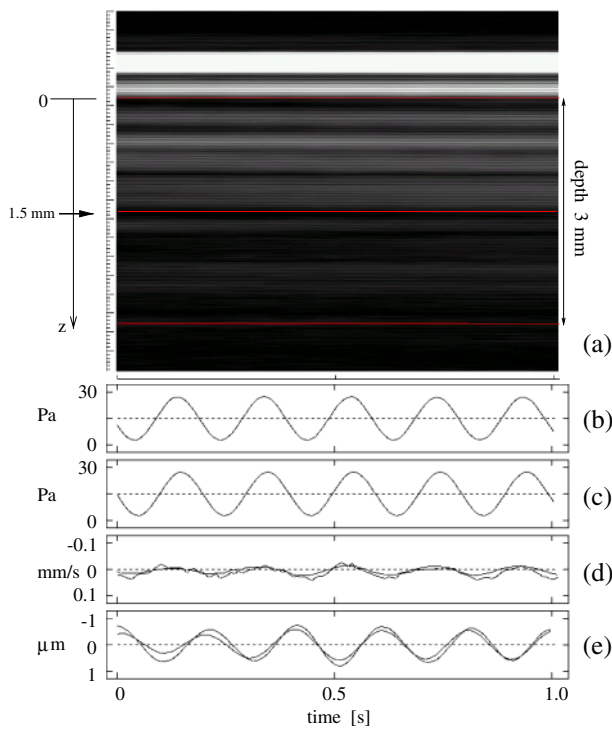


Fig. 6. (Color online) (a) M-mode image of an object. (b) Acoustic radiation pressure,  $P_{R1}(t)$ . (c) Acoustic radiation pressure,  $P_{R2}(t)$ . (d) Vibration velocities at 0 and 1.5 mm from the surface. (e) Displacements at 0 and 1.5 mm from the surface.

the ultrasound for actuation with a hydrophone (Force Institute MH-28-10), the amplitude of the focused sound pressure of  $p_0$  was obtained.

The vibration velocities,  $\{v_z(t)\}$ , at beam position  $x = 0$  and depths  $z = 0$  mm (surface) and 1.5 mm within the object actuated by the acoustic radiation force were measured by the ultrasonic *phased tracking method*, as shown in Fig. 6(d). By integrating velocities  $\{v_z(t)\}$ , the displacements,  $\{d_z(t)\}$ , at the depths  $z = 0$  mm and 1.5 mm were obtained as shown in Fig. 6(e). It was found that the object

was cyclically actuated at the frequency difference  $\Delta f = 5$  Hz at an amplitude of 1.5  $\mu$ m.

By applying the ultrasonic *phased tracking method* at every sampled points from the surface to 3 mm deep within the object, the spatial distributions of displacements,  $\{d_{x,z}(t)\}$ , were measured. Moreover, changes in thickness (strain),  $\{\Delta h_{x,z}(t)\}$ , were obtained as the spatial gradient of displacements calculated by applying the least-squares method to the displacement distribution in every region with a width of 1.5 mm in the depth direction. Spatially random variation of displacements was large, and it is difficult to obtain the change in thickness from the difference between the displacements of two points.

Figures 7 and 8 show the spatial distributions of displacements,  $\{d_{x,z}(t)\}$ , and changes in thickness,  $\{\Delta h_{x,z}(t)\}$ , during a cycle of acoustic radiation forces at distances between two focal points of 0 mm and 8 mm, respectively. The dashed lines in Figs. 7(c) and 8(c) show the time when each distribution is measured. In Figs. 7(a) and 8(a), the measured displacements,  $\{d_{x,z}(t)\}$ , are superimposed on the B-mode images using a color code shown at the bottom of Figs. 7(a) and 8(a). Blue and red correspond to the upward and downward displacements, respectively. In Figs. 7(b) and 8(b), the measured changes in thickness,  $\{\Delta h_{x,z}(t)\}$ , are superimposed on the B-mode images using a color code shown in the bottom of Figs. 7(b) and 8(b). Blue indicates a thinning region and red indicates a thickening one.

In Fig. 7(a), the downward displacements were generated at the surface of the object during the period when the acoustic radiation forces increased. The region around the surface of the object was displaced downward slightly more than a deep region because two acoustic radiation forces intersected at the surface. Therefore, in Fig. 7(b), the region around the surface became somewhat thinner when the applied acoustic radiation forces increased because the object was not compressed horizontally.

In Fig. 8(a), in the region (around a depth of 1.8 mm) where two acoustic radiation forces crossed, amplitudes of

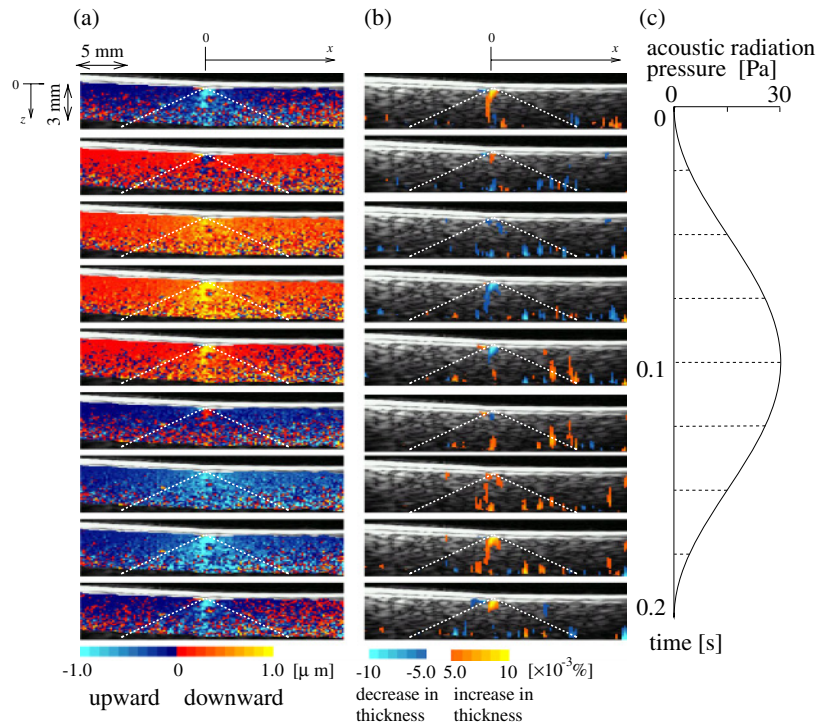


Fig. 7. (Color online) Experimental results from the phantom at a distance between two focal points of 0 mm. (a) Distribution of displacements,  $\{d_{x,z}(t)\}$ , inside the object. (b) Distribution of strain (changes in thickness),  $\{\Delta h_{x,z}(t)\}$ , inside the object. (c) Acoustic radiation force during one cycle.

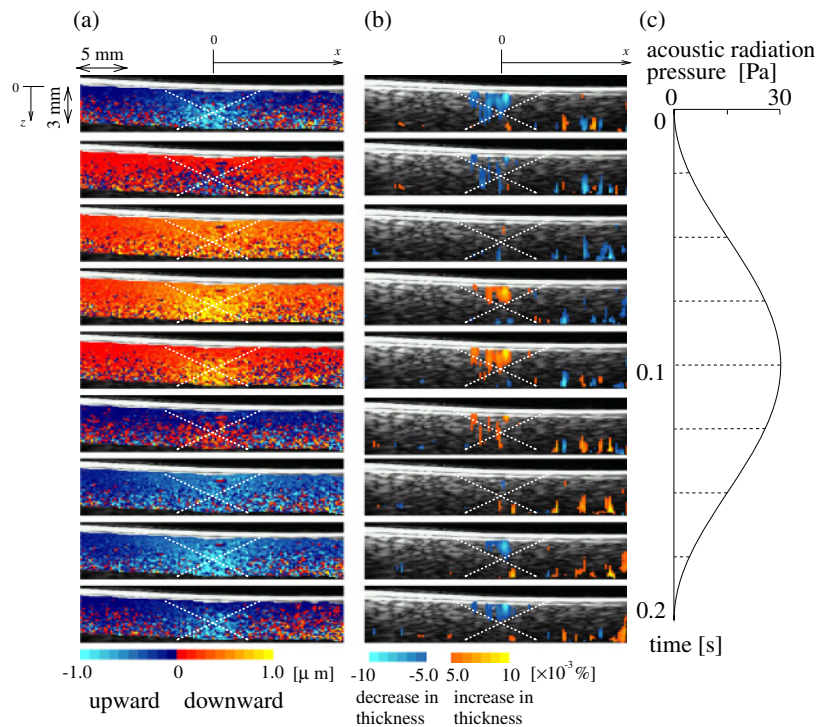


Fig. 8. (Color online) Experimental results from the phantom at a distance between two focal points of 8 mm. (a) Distribution of displacements,  $\{d_{x,z}(t)\}$ , inside the object. (b) Distribution of strain (changes in thickness),  $\{\Delta h_{x,z}(t)\}$ , inside the object. (c) Acoustic radiation force during one cycle.

displacements were larger than those in the other region. Although the region around the surface of the object was compressed in the horizontal direction by the horizontal components of the applied acoustic radiation forces, the region was displaced upward or downward unidirectionally because

the applied radiation forces have vertical components. The horizontal compression can be revealed by estimating the spatial distribution of the strain (change in thickness),  $\{\Delta h_{x,z}(t)\}$ , as shown in Fig. 8(b). In Fig. 8(b), the region around the midpoint between two focal points thickened

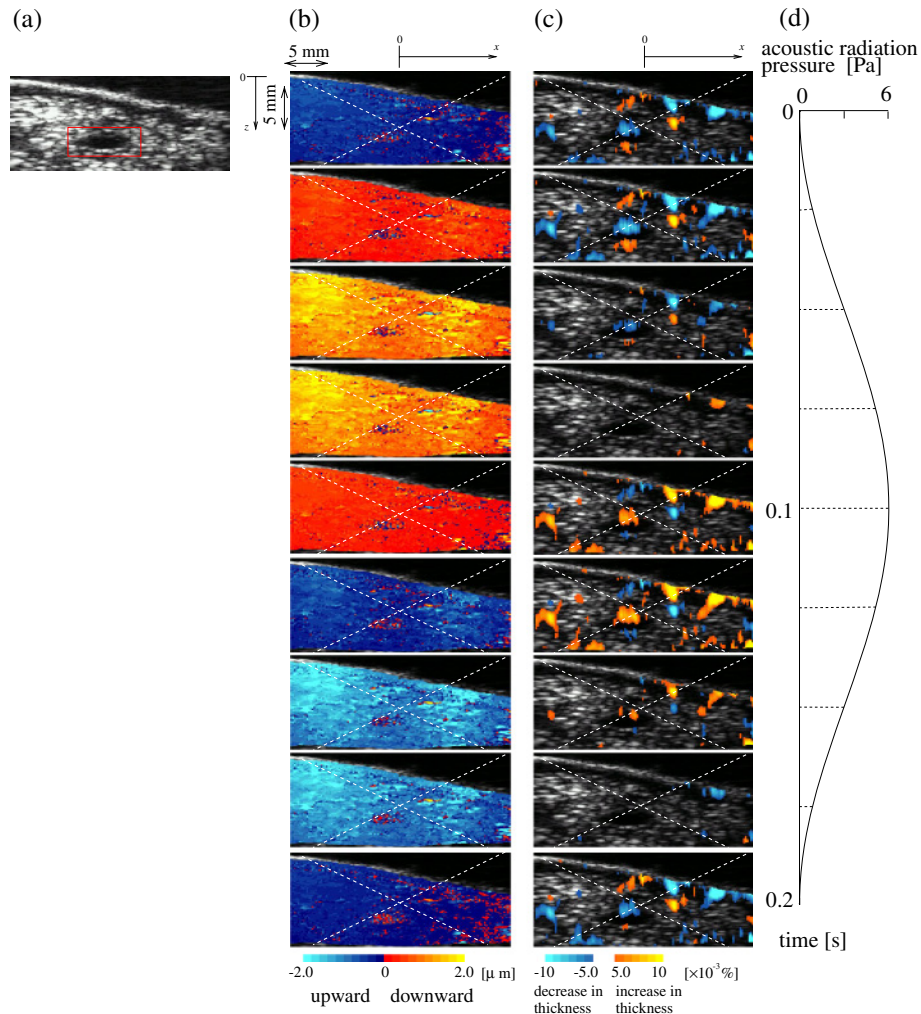


Fig. 9. (Color online) (a) B-mode image of porcine liver. (b) Distribution of displacements,  $\{d_{x,z}(t)\}$ , inside the porcine liver. (c) Distribution of strain (changes in thickness),  $\{\Delta h_{x,z}(t)\}$ , inside the porcine liver. (d) Acoustic radiation force during one cycle.

when the applied acoustic radiation forces increased. This result suggests that the object is actually compressed in the horizontal direction and is expanded in the vertical direction due to its incompressibility. From these results, it was found that strain inside the object was successfully generated specifically around the midpoint between two focal points.

#### 4.3 *In vitro* experiments using porcine liver

An *in vitro* experiment using porcine liver, which is softer than silicone gel, was conducted. In Figs. 7 and 8, the distance between two focal points is set at 8 mm. In this experiment, acoustic radiation forces were applied at a low intensity of 6 Pa compared with the basic experiments using silicone gel (about 1/5 of the intensity). This intensity complies with the safety standards for ultrasound.

Figure 9(a) shows a B-mode image of the porcine liver. There was an artery in the region which is surrounded by the red rectangle in Fig. 9(a). Figures 9(b) and 9(c) show the spatial distributions of displacements,  $\{d_{x,z}(t)\}$ , and strains (changes in thickness),  $\{\Delta h_{x,z}(t)\}$ , along each beam during a cycle of acoustic radiation forces shown by color codes indicated in the bottom of these figures. The dashed lines in Fig. 9(d) show the time when each distribution is displayed.

In Fig. 9(b), in spite of the fact that acoustic radiation

forces were applied at a low intensity, amplitude of displacements were larger than those of the silicone gel. In addition, as shown in Fig. 10, it was observed that a shear wave propagated to the outside from the region where acoustic radiation forces were radiated. The measured region in Fig. 10 was moved 10 mm in the horizontal direction in comparison with that in Fig. 9. The propagation of the shear wave was visualized because the liver is much softer than the gel.

In Fig. 10, the propagation velocity of the shear wave,  $c_s$ , is calculated as 1.3 m/s. By assuming the density of liver,  $\rho$ , to be  $1.0 \times 10^3$  kg/m<sup>3</sup> and the liver to be incompressible, shear modulus,  $G$ , is calculated by

$$G = \rho c_s^2. \tag{4.1}$$

The shear modulus,  $G$ , was determined to be 1.7 kPa, which is similar to that reported in literature.<sup>17)</sup> This result shows that it is possible to evaluate elasticity from the propagation speed of a shear wave.

In Fig. 9(c), large changes in thickness were generated in the region over the blood vessel. The region became thin when overall downward displacements were caused by acoustic radiation forces because the blood vessel was hard compared with liver tissue.

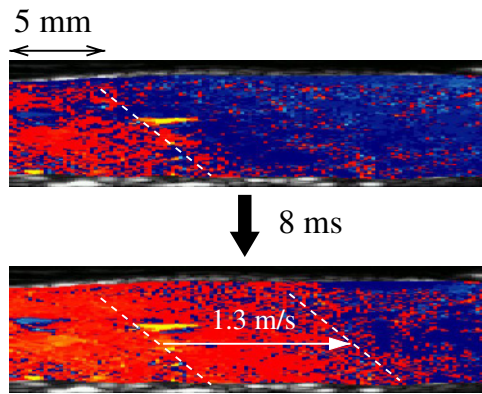


Fig. 10. (Color online) Propagation of shear wave in the porcine liver.

5. Discussion

In this study, the spatial distributions of displacements and changes in thickness caused by two acoustic radiation forces were measured with the ultrasonic *phased tracking method*. In this section, the applied acoustic radiation forces and resulting changes in thickness distribution are discussed. The region where the acoustic radiation force was over the half maximum is roughly illustrated in Fig. 11(a). Figure 11(a) shows the result when the focal points of two ultrasound beams for actuation were set at the same position. In this case, the resultant force from two acoustic radiation forces has almost only a downward component at the vicinity of the surface, and the resulting downward displacement during the increase of acoustic radiation forces is shown in the experimental results in Fig. 7. Figure 11(b) illustrates the acoustic radiation force when the distance between focal points at the surface was set to 8 mm. Two ultrasound beams crossed each other at a depth of 1.8 mm from the surface. In this case, the region between two ultrasound beams for actuation was compressed along the horizontal axis, and the region which vertically thickens during the increases of acoustic radiation forces is shown by the basic experiment using a phantom.

As shown in Fig. 8, in a homogeneous object, strain inside the object was successfully generated by applying two acoustic radiation forces from two opposite horizontal directions. Therefore, the elastic properties of a homogeneous object, such as large muscle, can be assessed from the magnitude of the deformation generated. However, in an inhomogeneous object, for example, a blood vessel in liver tissue as shown in Fig. 9, the strain is not generated in the same manner as in the basic experiment because of the complex deformation generated. The displacement distribution generated also depends on the elasticity and elastic inhomogeneity of an object, and such dependence should be further investigated in future work.

6. Conclusions

In this study, the spatial distributions of displacements and changes in thickness inside an object were generated by two acoustic radiation forces and they were measured by the ultrasonic *phased tracking method*. It was shown that strain could be generated using two acoustic radiation forces. These results show the potential of the proposed method for

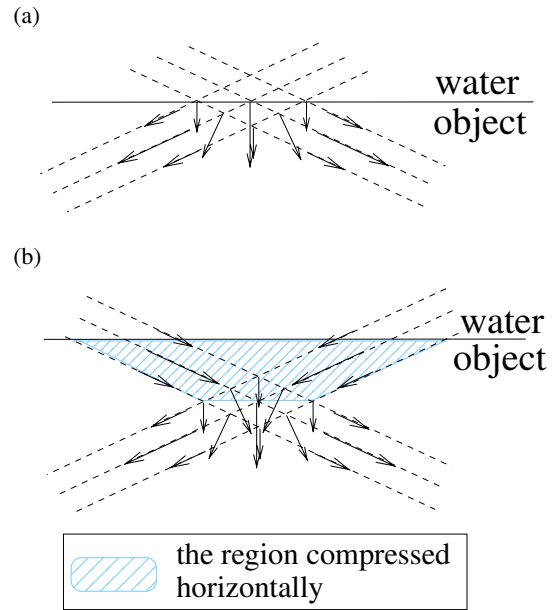


Fig. 11. (Color online) Illustrations of (a) resultant radiation forces when focal points were set at the same position and (b) resultant radiation forces when the distance of focal points between ultrasound beams for actuation was set to 8 mm.

evaluation of the change in elastic spatial properties of muscle. Moreover, this method could be useful for the measurement of elastic properties of tissues, for example, liver and breast tissue, which require an external force to be deformed.

- 1) M. Fatemi, L. E. Wold, A. Alizod, and J. F. Greenleaf: *IEEE Trans. Med. Imaging* **21** (2002) 1.
- 2) M. Fatemi and J. F. Greenleaf: *Proc. Natl. Acad. Sci. U.S.A.* **96** (1999) 6603.
- 3) K. Nightingale, M. S. Soo, R. Nightingale, and G. Trahey: *Ultrasound Med. Biol.* **28** (2002) 227.
- 4) G. E. Trahey, M. L. Palmeri, R. C. Bentley, and K. R. Nightingale: *Ultrasound Med. Biol.* **30** (2004) 1163.
- 5) B. J. Fahey, K. R. Nightingale, R. C. Nelson, M. L. Palmeri, and G. E. Trahey: *Ultrasound Med. Biol.* **31** (2005) 1185.
- 6) Japan Society of Ultrasonics in Medicine: *Cho-onpa Igaku* **11** (1984) 41 [in Japanese].
- 7) H. Hasegawa, M. Takahashi, Y. Nishio, and H. Kanai: *Jpn. J. Appl. Phys.* **45** (2006) 4706.
- 8) K. Michishita, H. Hasegawa, and H. Kanai: *Jpn. J. Appl. Phys.* **42** (2003) 4608.
- 9) H. Kanai, M. Sato, Y. Koiwa, and N. Chubachi: *IEEE Trans. Ultrason. Ferroelectr. Freq. Control* **43** (1996) 791.
- 10) H. Kanai, H. Hasegawa, N. Chubachi, Y. Koiwa, and M. Tanaka: *IEEE Trans. Ultrason. Ferroelectr. Freq. Control* **44** (1997) 752.
- 11) G. R. Torr: *Am. J. Phys.* **52** (1984) 402.
- 12) H. Kanai, K. Sugimura, Y. Koiwa, and Y. Tsukahara: *Electron. Lett.* **35** (1999) 949.
- 13) J. Inagaki, H. Hasegawa, H. Kanai, M. Ichiki, and F. Tezuka: *Jpn. J. Appl. Phys.* **45** (2006) 4732.
- 14) T. Kaneko, H. Hasegawa, and H. Kanai: *Jpn. J. Appl. Phys.* **46** (2007) 4881.
- 15) H. Kanai, H. Hasegawa, and K. Imamura: *Jpn. J. Appl. Phys.* **45** (2006) 4718.
- 16) H. Yoshiara, H. Hasegawa, H. Kanai, and M. Tanaka: *Jpn. J. Appl. Phys.* **46** (2007) 4889.
- 17) E. J. Chen, J. Novakofski, W. K. Jenkins, and W. D. O'Brien, Jr.: *IEEE Trans. Ultrason. Ferroelectr. Freq. Control* **43** (1996) 191.